

# Antiviral Lipid Nanocarrier Loaded with Remdesivir Effective Against SARS-CoV-2 in vitro Model

Woo-Jin Jeon<sup>1,\*</sup>, Hong-Ki Lee<sup>2,3,\*</sup>, Young-Guk Na<sup>1</sup>, Minwoo Jung<sup>1</sup>, Su-Cheol Han<sup>2</sup>, Jeong Ho Hwang<sup>2</sup>, Eunhye Jung<sup>4</sup>, Dasom Hwang<sup>4</sup>, Jin Soo Shin<sup>4</sup>, Cheong-Weon Cho<sup>1</sup> 

<sup>1</sup>College of Pharmacy and Institute of Drug Research and Development, Chungnam National University, Daejeon, 34134, Republic of Korea; <sup>2</sup>Center for Companion Animal New Drug Development, Jeonbuk Branch, Korea Institute of Toxicology (KIT), Jeongeup, Jeollabuk-do, 53212, Republic of Korea; <sup>3</sup>Human Health Risk Assessment Center, Jeonbuk Branch, Korea Institute of Toxicology (KIT), Jeongeup, Jeollabuk-do, 53212, Republic of Korea; <sup>4</sup>Infectious Diseases Therapeutic Research Center, Korea Research Institute of Chemical Technology, Daejeon, Republic of Korea

\*These authors contributed equally to this work

Correspondence: Jin Soo Shin, Infectious Diseases Therapeutic Research Center, Korea Research Institute of Chemical Technology, Daejeon, Republic of Korea, Email [jsshin@kriict.re.kr](mailto:jsshin@kriict.re.kr); Cheong-Weon Cho, College of Pharmacy and Institute of Drug Research and Development, Chungnam National University, 99 Daehak-ro, Yuseong-gu, Daejeon, 34134, Republic of Korea, Email [chocw@cnu.ac.kr](mailto:chocw@cnu.ac.kr)

**Introduction:** The ongoing SARS-CoV-2 pandemic has affected public health, the economy, and society. This study reported a nanotechnology-based strategy to enhance the antiviral efficacy of the antiviral agent remdesivir (RDS).

**Results:** We developed a nanosized spherical RDS-NLC in which the RDS was encapsulated in an amorphous form. The RDS-NLC significantly potentiated the antiviral efficacy of RDS against SARS-CoV-2 and its variants (alpha, beta, and delta). Our study revealed that NLC technology improved the antiviral effect of RDS against SARS-CoV-2 by enhancing the cellular uptake of RDS and reducing SARS-CoV-2 entry in cells. These improvements resulted in a 211% increase in the bioavailability of RDS.

**Conclusion:** Thus, the application of NLC against SARS-CoV-2 may be a beneficial strategy to improve the antiviral effects of antiviral agents.

**Keywords:** remdesivir, nanostructured lipid carrier, antiviral effect, SARS-CoV-2, virus entry

## Introduction

At the end of 2019, coronavirus disease (COVID-19) emerged and began to spread worldwide. The World Health Organization (WHO) officially declared the COVID-19 outbreak a pandemic in March 2020.<sup>1</sup> COVID-19 is caused by severe acute respiratory syndrome coronavirus 2 (SARS-CoV-2), which has high transmissibility and infectivity. To date, over 150 million cases have been confirmed, with three million deaths worldwide.<sup>2</sup> The COVID-19 pandemic is still ongoing and has greatly affected public health, the economy, and society. Despite an urgent need for treatment, there are currently no specific or effective agents against SARS-CoV-2.

SARS-CoV-2, which belongs to the genus *Betacoronavirus*, is a single-stranded RNA virus measuring less than 100 nm that has a large number of glycosylated spike proteins (S-proteins) on its surface.<sup>3</sup> These S-proteins play an important role in virus entry by binding to the angiotensin-converting enzyme 2 (ACE2) and CD147 receptors of the host cell.<sup>4,5</sup> Following virus entry into the host cell, viral RNA is released and translated by the ribosome. The translated polyproteins pp1a/pp1ab are then cleaved by the protease, after which the replicase–transcriptase complex is formed; it is this complex that initiates viral RNA synthesis.<sup>6</sup> Virus particles, which are formed by the structural protein and viral RNA, are then released from the host cell. This increases the secretion of inflammatory cytokines by macrophages and monocytes,<sup>7</sup> and leads to a cytokine storm that worsens the inflammatory state of the host.<sup>8</sup> Moreover, the secretion of vascular endothelial growth factor (VEGF), monocyte chemoattractant protein–1 (MCP-1), and IL-8 by the cytokine storm increases vascular permeability and leakage, making the host susceptible to immune and pulmonary dysfunctions.<sup>8</sup>

Various novel or repurposed agents for the treatment of SARS-CoV-2 infection are under investigation.<sup>9,10</sup> Several classes of agents, including antiviral agents, ACE2 inhibitors, neutralizing antibodies, and immunomodulators, have been evaluated *in vitro* and *in vivo*.<sup>11–16</sup> One of these, the drug remdesivir (RDS, Veklury<sup>®</sup>) was approved by the US Food and Drug Administration (FDA) for the treatment of COVID-19 in patients requiring hospitalization.<sup>17</sup> RDS, a monophosphoramidate prodrug of an adenosine analog, was originally developed for the treatment of Ebola virus and has been since found to inhibit multiple RNA viruses.<sup>18–20</sup> The antiviral mechanism of RDS is mediated in two ways. For one, a non-canonical RNA nucleotide is inserted into the RNA strand; because this nucleotide is not recognized by RNA-dependent RNA polymerase (RdRp) during replication, chain elongation is terminated.<sup>21</sup> Alternatively, viral replication is inhibited when RDS binds to RdRp, thus blocking viral RNA from entering the active site of RdRp.<sup>22</sup> Since RDS is mostly metabolized and cleared by first-pass metabolism, RDS was developed as an injectable formulation.<sup>23</sup> However, it exhibits poor solubility in water; thus, the commercial product (Veklury<sup>®</sup>) contains sulfobutylether-beta-cyclodextrin (SBECD) as an excipient to improve solubility.<sup>24</sup> Although SBECD is commonly used for the improvement of the water solubility and bioavailability of drugs, it is renally cleared and may accumulate in patients with reduced renal function.<sup>23</sup>

Over the last decade, nanotechnology has become a growing strategy for improving the bioavailability and safety of drugs. A drug delivery system (DDS) developed using nanotechnology avoids immune recognition and overcomes other biological barriers in order to efficiently deliver drugs.<sup>25</sup> Nanostructured lipid carriers (NLCs) are a new generation of lipid-based nanoparticles. The NLC consists of both solid and liquid lipids and forms structureless matrices, which leads to improved drug storage.<sup>26</sup> Additionally, owing to the improved drug capacity of NLCs, drug release can be controlled. Therefore, using a DDS to deliver RDS would improve the bioavailability and renal safety of this drug. Moreover, nanosystems have advantages with regard to SARS-CoV-2 infection and treatment management.<sup>27–29</sup> Nanosystems could be useful in the prevention and diagnosis of SARS-CoV-2 infection, and in the targeted delivery of therapeutics.<sup>27</sup> In particular, novel nanosystem-based therapeutics could avoid off-targeting and unnecessary drug ingestion.<sup>28</sup> Thus, using nanotechnology for RDS would improve its efficacy by working as an efficient DDS.

This study aimed to develop RDS-loaded-NLC (RDS-NLC) to improve the efficacy and bioavailability of RDS. We hypothesized that NLC would affect the SARS-CoV-2 life cycle in the host cell; thus, we evaluated the therapeutic potential of NLC to determine whether it improves the therapeutic effects of RDS or provides a prophylactic effect.

## Materials and Methods

### Materials

RDS (GS-5734) was purchased from MedChemExpress (St. Louis, MO, USA). Glycerol monostearate (GMS) was purchased from KANTO CHEMICAL Co. Inc. (Tokyo, Japan). National formulary grade glyceryl caprylate/caprate (Capmul MCM) was purchased from ABITEC Corporation (Cleveland, OH, USA). Polyoxyethylene 40 stearate (Myrj52) was a gift from CRODA, Inc. (Snaith, UK). Primary and secondary antibodies against IFA were purchased from Genetex (Irvine, CA, USA) and Thermo Fisher Scientific (Waltham, MA, USA), respectively. HPLC-grade acetonitrile (ACN) and methanol were purchased from Samchun Chemical Co. Ltd. (Pyungtaek, Korea).

### Synthesis of Remdesivir-Loaded Nanostructured Lipid Carriers

RDS-NLC was synthesized using a hot melting method with GMS, Capmul MCM, and Myrj52. Briefly, RDS (5 mg) and lipids (105 and 45 mg of GMS and Capmul MCM, respectively) were mixed and heated at 80°C to prepare the lipid phase. To prevent solidification of the lipid phase, the aqueous phase was prepared by dissolving Myrj52 (100 mg) in distilled water (10 mL) at 80°C. The aqueous phase was added to the lipid phase and the mixture was homogenized at 15,000 × g for 2 min using a homogenizer (T 25 digital ULTRA-TURRAX<sup>®</sup>, IKA, Wilmington, NC, USA). The homogeneous emulsion was then sonicated at 35% amplitude for 8 min (5/3 s on-off time cycle) using an ultrasonicator (Vibra-Cell<sup>™</sup>; SONICS<sup>®</sup>, Newtown, CT, USA). The ultrasonicated emulsion (of RDS-NLCs) was placed in an ice bath

**Table 1** Composition of the Blank-NLC and RDS-NLC

Formulations	RDS (mg)	GMS (mg)	Capmul MCM (mg)	Myrj52 (mg)	D.W (mL)
Blank-NLC	-	105	45	100	10
RDS-NLC	5	105	45	100	10

and cooled at 4°C. Blank NLCs were prepared using the method described above, but without RDS. Table 1 lists the composition of the RDS-NLC.

## Physicochemical Characterization of Remdesivir-Loaded Nanostructured Lipid Carriers

### Analysis of Particle Size, Zeta Potential, and Morphology

The particle size, polydispersity index (PDI), and zeta potential of the RDS-NLCs were evaluated using an electrophoretic laser scattering (ELS) analyzer (ELSZ-2000 series; Otsuka Electronics, Osaka, Japan). Briefly, RDS-NLCs were diluted in distilled water (x10) and the particle size and PDI were measured 50 times. All measurements were performed in triplicate.

The morphology of the RDS-NLCs was observed using a transmission electron microscope (Tecnai G2 F30; FEI Company, Hillsboro, OR, USA). Briefly, RDS-NLCs were diluted in distilled water, 2 µL of RDS-NLCs was placed on the grid, and the morphology was observed using a transmission electron microscope (TEM).

### Evaluation of the Encapsulation Efficiency and Drug Loading Capacity of Remdesivir-Loaded Nanostructured Lipid Carriers

Encapsulation efficiency (EE) and drug loading capacity (DC) were evaluated using ultrafiltration. Briefly, 1 mL of RDS-NLCs was added to a polypropylene tube and centrifuged at 15,000 × g for 15 min at 4°C. The supernatant was collected and then diluted in ACN. The amount of RDS in the supernatant was measured using ultra-performance liquid chromatography - tandem mass spectrometry (UPLC-MS/MS) (1290 series; 6495 triple q; Agilent Technologies, Santa Clara, CA, USA). EE and DL were calculated using the following equations:

$$EE(\%) = (\text{Total drug amount (mg)} - \text{Amount of RDS in supernatant (mg)}) / (\text{Total drug amount (mg)}) \times 100$$

$$DC(\%) = (\text{Total drug amount (mg)} - \text{Amount of RDS in supernatant (mg)}) / (\text{Total NLC amount (mg)}) \times 100$$

### Differential Scanning Calorimetry, Fourier Transform-Infrared Spectroscopy, and X-Ray Diffraction Analyses of Remdesivir-Loaded Nanostructured Lipid Carriers

Differential scanning calorimetry (DSC), Fourier transform-infrared spectroscopy (FT-IR), and x-ray diffraction (XRD) analyses were employed to evaluate changes in the crystalline form of the NLCs and interactions among their components. For DCS analysis, 2 mg of RDS-NLC was placed in aluminum pans and heated from 30°C to 150°C. The heating rate was set at 10°C /min. DSC thermograms were measured and recorded using a DSC instrument (DSC N-650; SCINCO, Seoul, Korea).

For the FT-IR analysis, the interaction between RDS and the formulation components was evaluated using an FT-IR spectrometer (ALPHA-P; Bruker, Billerica, MA, USA). The spectra were set from 4000 to 500 cm<sup>-1</sup>.

The changes in the crystalline form of RDS-NLCs were evaluated using an X-ray diffractometer (D8 ADVANCE; Bruker, Billerica, MA, USA). The diffraction angle was 2θ, and the scanning speed was 0.02°/s in the range of 5–50°.

### In vitro Release Properties of Remdesivir-Loaded Nanostructured Lipid Carriers

The release properties of RDS and RDS-NLC were evaluated in PBS (pH 7.4) with 2 w/v% sodium lauryl sulfate (SLS) using a modified dialysis bag membrane diffusion technique.<sup>30</sup> The dialysis membrane release technique was used to evaluate the release properties. RDS and RDS-NLC (as 2 mg of RDS) were placed into a 7 kDa molecular weight cut off (MWCO) dialysis membrane (Viskase, Inc., Lombard, IL, USA). The dialysis membranes were then placed in 50 mL of medium while stirring at 150 rpm. Samples were taken at 0.08, 0.25, 0.5, 1, 2, 4, 6, 8, 12, 24, and 48 h. After sampling,

the same volumes of medium were inoculated. All samples were determined using HPLC to evaluate the release profile of RDS and RDS-NLC.

## Evaluation of Cellular Uptake of Remdesivir-Loaded Nanostructured Lipid Carriers

### Cell Culture

Vero E6 (ATCC<sup>®</sup> CRL-1586), a monkey kidney epithelial cell line, was used to evaluate the cellular uptake of RDS-NLCs. Vero cells were maintained in Dulbecco's modified Eagle's medium (DMEM) supplemented with 10% fetal bovine serum (FBS), 100 units/mL penicillin, and 100 µg/mL streptomycin at 37°C and 5% CO<sub>2</sub>.

### The Cellular Uptake of Remdesivir-Loaded Nanostructured Lipid Carriers

The cellular uptake of RDS-NLCs was evaluated by measuring the amount of RDS in Vero cells. Briefly, cells were seeded in 12-well plates at a concentration of  $1 \times 10^5$  cells/well. The plates were then incubated at 37°C for 24 h. After incubation, 5 µM RDS solution or RDS-NLC was added to each well. After 24 h of incubation, the plate was washed three times with cold PBS and 0.5 mL of lysis buffer (CETi lysis buffer, TransLab, Daejeon, Korea) was added to each well. The cell lysate was then transferred into a tube, and methanol was added to extract RDS. The cell lysate was shaken at 1000 rpm for 10 min and centrifuged at  $15,000 \times g$  for 20 min at 4°C. The supernatant was injected into the UPLC-MS/MS system, and the amount of RDS was measured. The amount of RDS in the Vero cells was normalized using the BCA assay.

### Immunofluorescence Imaging of Remdesivir-Loaded Nanostructured Lipid Carriers in Vero Cells

Fluorescence imaging was used to evaluate the amount of RDS and RDS-NLC in Vero E6 cells. Briefly, Vero E6 cells were seeded on a 4-chamber glass slide (SPL, Pocheon, Republic of Korea) at a density  $1 \times 10^5$  cells/chamber and cultured for 24 h in a 5% CO<sub>2</sub> incubator. After they were cultured, the cells were treated with 5 µM of Coumarin-6 (C6) solution (as RDS) and C6 labeled RDS-NLC for 24 h. After treatment, the cells were washed with cold PBS 3 times and fixed with 4 w/v% paraformaldehyde (PFA) for 30 min at RT. After fixation, the cells were stained with mounting solution (with DAPI) and observed.

To visualize RDS-NLC in SARS-CoV-2 infected cells, immunofluorescence microscopy was used. Briefly, Vero cells were seeded on a 4-chamber glass slide (SPL, Korea) at a density of  $1 \times 10^5$  cells per chamber and cultured overnight at 37°C in a 5% CO<sub>2</sub> incubator. Cells were infected with SARS-CoV-2 at a multiplicity of infection (MOI) of 1 for 1 h at 37°C in a 5% CO<sub>2</sub> incubator, washed with PBS, and treated with 1 µM RDS-NLC for 24 h. Cells were fixed with 4% (w/v) paraformaldehyde (PFA) for 30 min at room temperature (RT), permeabilized with 0.1% bovine serum albumin (BSA) in 0.03% Triton X-100 for 10 min at RT, and blocked with 0.03% Triton X-100 containing 10% normal goat serum (NGS, Thermo Fisher Scientific) for 30 min at RT. Cells were stained with anti-S (Genetex) and Alexa Fluor 647-conjugated goat anti-mouse IgG secondary antibodies (Invitrogen, Waltham, MA, USA), whereas cellular nuclei were stained with 4',6-diamidino-2-phenylindole (DAPI, Invitrogen). Images were analyzed using a confocal microscope (Zeiss LSM 710, Germany).

## Antiviral Effects of Remdesivir-Loaded Nanostructured Lipid Carriers in SARS-CoV-2 Infected Cells

### Cells and Viruses

Vero E6 (ATCC<sup>®</sup> CRL-1586) cells were maintained in Dulbecco's modified Eagle's medium (DMEM; HyClone) supplemented with 10% FBS (HyClone) at 37°C in a 5% CO<sub>2</sub> incubator. Patient-derived isolate SARS-CoV-2 (hCoV-19/Korea/KCDC-06/2020, hCoV-19/Korea/KDCA51463/2021, hCoV-19/Korea/KDCA55905/2021, hCoV-19/Korea/KDCA119861 / 2021) was kindly provided by the Korea Disease Control and Prevention Agency (KDCA, Osong, Republic of Korea), and the working virus stock was propagated in Vero E6 cells.<sup>31</sup> The virus-containing supernatants were collected, clarified by centrifugation, and aliquots were stored at -80°C until further use. Viral stocks were titrated by plaque assays using Vero E6 cells as previously described. All experiments using infectious SARS-CoV-2 were performed in a biosafety level-3 facility at the Korea Research Institute of Chemical Technology (KRICT), Daejeon, Republic of Korea.

### Antiviral Activity Assay

A CPE-based assay was used to evaluate the antiviral activities of RDS and RDS-NLCs in Vero E6 cells, as previously described but with modifications.<sup>32</sup> Briefly, Vero E6 cells were seeded at a density of  $1 \times 10^4$  cells per well in 96-well plates. The next day, after treatment with various concentrations of each drug, cells were infected with SARS-CoV-2 at an MOI of 0.05 for 72 hours. Cell viability at the endpoint was measured using the CellTiter 96<sup>®</sup> AQueous One Solution Cell Proliferation Assay (MTS, Promega, Madison, WI, USA). Absorbance was measured at 490 nm (A490) using a Synergy<sup>™</sup> H1 multi-mode microplate reader (BioTek, Winooski, VT, USA). To determine the EC<sub>50</sub> (half effective concentration) and CC<sub>50</sub> (half cytotoxic concentration), GraphPad Prism 9 (GraphPad Software, USA) was used, and was set to the following non-linear regression equation: log (inhibitor) vs response-variable slope (four parameters curve).

### Viral Plaque Assay

To determine the infectious SARS-CoV-2 titers, a plaque assay was performed.<sup>32</sup> Briefly,  $2 \times 10^5$  Vero E6 cells/well were added to 48-well plates and incubated overnight at 37°C. The supernatants were treated with various concentrations of each drug after harvesting, and serially diluted (10-fold) test samples were used to infect cells. After incubation for 1 h at 37°C for adsorption, cells were washed with PBS or plain DMEM, and overlay media with DMEM containing 0.8% agarose was added. After incubation for 72 h at 37°C, cells were stained with 0.05% crystal violet solution for plaque-forming staining and plaque counting, and analyses were performed using ImmunoSpot (Cellular Technology Ltd., Shaker Heights, OH, USA).

### Reverse Transcription-Quantitative Polymerase Chain Reaction Assay

For intracellular viral RNA quantification, RT-qPCR was performed.<sup>33</sup> Briefly, total cellular RNA was extracted from cell lysates using an RNeasy mini kit (Qiagen, Hilden, Germany) according to the manufacturer's instructions. The SARS-CoV-2 viral RNA load was quantified using a SuperScript III Platinum<sup>®</sup> SYBR<sup>®</sup> Green One-Step RT-PCR kit (Invitrogen), with a primer set targeting the SARS-CoV-2 receptor-binding domain (RBD) gene (sense 5'-CAATG GTTTAACAGGCACAGG-3' and antisense 5'-CTCAAGTGTCTGTGGAT CACG-3'). Relative SARS-CoV-2 viral RNA expression levels were calculated using the  $\Delta\Delta CT$  method, and  $\beta$ -actin was used as an endogenous control.

## Effects of Remdesivir-Loaded Nanostructured Lipid Carriers on the Life Cycle of SARS-CoV-2

To determine the mode of action of RDS-NLC, a time-of-drug-addition assay was performed.<sup>32</sup> Briefly, Vero E6 cells were seeded at a density of  $2 \times 10^5$  cells per well in 12-well plates and incubated overnight at 37°C and 5% CO<sub>2</sub>. Cells were infected with SARS-CoV-2 at 1 MOI and independently treated with 10  $\mu$ M RDS and 2  $\mu$ M RDS-NLC at -2 (pre), 0 (co), and 2 h (post). Culture supernatants were harvested 24 h post-infection to measure the plaque assay for infectious SARS-CoV-2 titers.

## Pharmacokinetic Evaluation of Remdesivir-Loaded Nanostructured Lipid Carriers

### Animal Experiments

The pharmacokinetic properties of RDS-NLCs were evaluated in male Sprague Dawley rats (SD rats), aged 7 weeks. Animals were purchased from Nara-Biotec (Seoul, Korea). The rats weighed 250–300 g and were housed under a 12 h dark/light cycle at 22°C and 55% relative humidity. Food and water were provided *ad libitum*. All animal studies were performed in accordance with the “Guidelines for Use of Animals” established by the Chungnam National University Institutional Animal Care and Use Committee (Daejeon, Korea). This study was approved by the Chungnam National University Institutional Animal Care and Use Committee (No. 202009-CNU-130).

Animals (12 rats) were acclimated for a week and divided into two groups: RDS solution and RDS-NLC (6 rats for each group). They fasted for 12 h before the injection of RDS or RDS-NLC. The RDS solution (dissolved in sulfobutylether- $\beta$ -cyclodextrin) and RDS-NLCs were intravenously injected into rats at a dose of 10 mg/kg. After the injection of RDS solution and RDS-NLCs, whole blood was collected into an EDTA tube at predetermined time points

(0, 0.09, 0.25, 0.5, 1, 2, 4, 6, 8, and 12 h). Blood was centrifuged at  $1500 \times g$  for 10 min, and plasma was collected. Plasma samples were stored at  $-70^{\circ}\text{C}$  prior to RDS analysis.

### Remdesivir and Nucleoside Metabolites in Plasma Samples

RDS is a prodrug that is metabolized into several metabolites. First, RDS is rapidly metabolized into an intermediate alanine metabolite (GS-704277), which is subsequently transformed into the nucleoside monophosphate form. The nucleoside monophosphate form is converted to either a pharmacologically active triphosphate form (GS-443902) or nucleoside metabolite (GS-441524), and GS-441524 was reported to exhibit a more persistent plasma level. Thus, we determined the concentrations of RDS and GS-441524 in plasma samples.

RDS and nucleoside metabolites were extracted from rat plasma using the liquid-to-liquid extraction (LLE) method, and the amount of RDS and metabolites in the plasma was determined using UPLC-MS/MS. Briefly, 100  $\mu\text{L}$  of plasma was dispersed into a tube, and 300  $\mu\text{L}$  of internal standard solution (IS, carbamazepine 10 ng/mL in methanol) was added. The mixture was then shaken for 10 min and centrifuged at  $15,000 \times g$  for 10 min at  $4^{\circ}\text{C}$ . The supernatant (100  $\mu\text{L}$ ) was filtered through a syringe filter (0.22  $\mu\text{m}$ ). The filtered supernatant (2  $\mu\text{L}$ ) was injected into the UPLC-MS/MS system.

To validate the bioanalytical method for RDS and GS-441524, rat plasma was spiked with RDS or GS-441524 and the precision/accuracy (inter- and intra-day) of the bioanalytical method was evaluated.

### Ultra-Performance Liquid Chromatography-Tandem Mass Spectrometry

To determine RDS and GS-441524 in plasma, UPLC-MS/MS (Agilent 1290 series and 6495 Triple Quad system, Agilent) was used, and the bioanalytical method for both RDS and GS-441524 was partially validated using rat plasma. Kinetex<sup>®</sup> 2.6  $\mu\text{m}$  XB-C18 100 $\text{\AA}$  column (50  $\times$  2.1 mm, 2.6  $\mu\text{m}$ ; Phenomenex, Torrance, CA, USA) was used, and the mobile phase consisted of 5 mM ammonium acetate aqueous solution (A) and HPLC-grade methanol (B). The gradient elution was set as 0–0.3 min: 0%, 0.3–2.3 min: 0 to 60%, 2.3–2.4 min: 60 to 70%, 2.4–3.3 min: 70%, 3.3–3.32 min: 70 to 0%, and 3.32–4.3 min: 0%; and the flow rate was 0.4 mL/min. RDS, GS-441524, and the IS ( $m/z = 602.2$ , 291.2, and 273, respectively) were observed at  $m/z$  202.2, 200.2 and 194, respectively. The gas temperature and flow rate were set at  $290^{\circ}\text{C}$  and 11 L/min, respectively. The entrance voltage was set to 5 kV. The optimized collision energies were 19 and 20 eV for GS-441524 and IS, respectively.

### Statistical Analysis

Data are expressed as mean  $\pm$  standard deviation (SD). Data were analyzed using a two-tailed unpaired Student's *t*-test and one-way analysis of variance ANOVA. Statistical significance was set as  $P < 0.05$ . Pharmacokinetic parameters for intravenous injection were determined individually as a non-compartmental model using WinNonlin 8.1 software (Pharsight, Princeton, NJ, USA). Statistical comparison of PK parameters was performed using Student's *t*-test.

## Results and Discussion

### Characterization of Remdesivir-Loaded Nanostructured Lipid Carriers

In the application of nanotechnology to drug delivery, it is important to understand the relationship between the physicochemical properties of nanoparticles and their bioactivity. Thus, we evaluated the physicochemical properties of RDS-NLCs to determine the influence of the characteristics of the nanoparticles on their bioactivity.

#### Analysis of Particle Size, Zeta Potential, and Morphology

The size and heterogeneity of the nanoparticles play an important role in their delivery efficiency and in the fate of the drug in vivo. In particular, the size of the nanoparticles can directly affect their interactions with the cell membrane, including interactions such as adhesion, endocytosis, and membrane disruption. Therefore, the cellular internalization of nanoparticles strongly depends on their size. While there is no limit or standard range of size for the cellular internalization of nanoparticles, it has been reported that diameters of approximately 60 nm are optimal for active uptake in the cell.<sup>34</sup> However, nanoparticles larger than 200 nm tend to activate the complement system and are cleared via the reticuloendothelial system in the kidney or liver.<sup>35</sup> Moreover, nanoparticles  $<10$  nm are prone to filtration via the kidney;

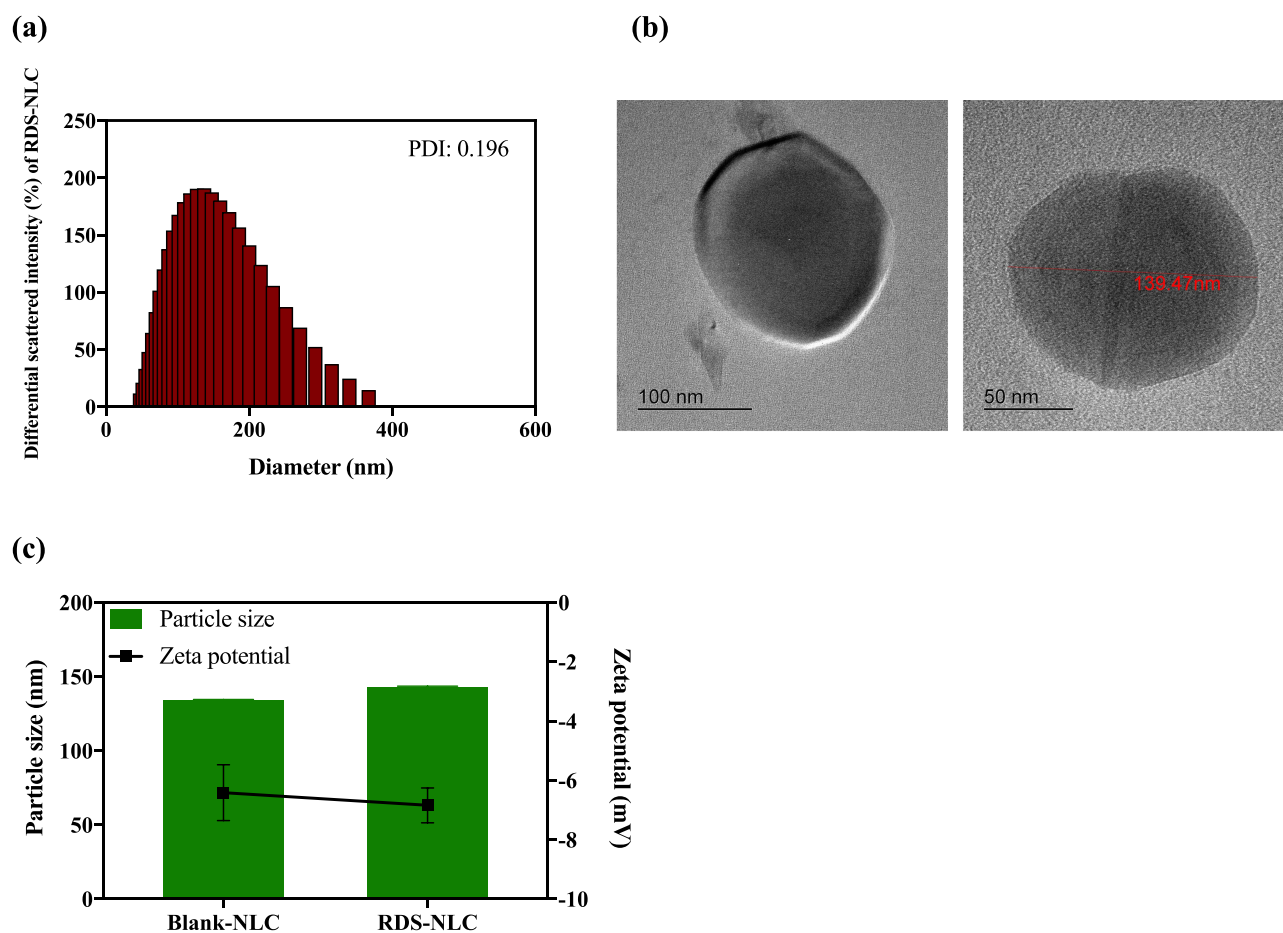


**Figure 1** Physicochemical properties of RDS-NLC. (a) Size and particle size distribution and (b) Transmission electron microscope images of RDS-NLC. (c) Particle size and zeta potential of Blank-NLC and RDS-NLC.

thus, nanoparticles ranging between 10 and 200 nm are sufficient to enhance the permeability and retention (EPR) effect and avoid rapid renal filtration or clearance by the reticuloendothelial system.<sup>34,36</sup>

We developed RDS-NLC using the hot melting method, previously published by our team.<sup>37</sup> The size of RDS-NLC, developed using glycerol monostearate (GMS, lipid), Capmul MCM, and Myrj52 (surfactant), was  $143.00 \pm 0.60$  nm (Figure 1). TEM observations revealed the spherical shape of NLC (Figure 1b), and the size distribution was evaluated by calculating the polydispersity index (PDI). The PDI of these RDS-NLCs was 0.196, indicating its homogeneity. A narrow PDI and a homogeneous hydrodynamic size distribution improve the safety and efficacy of nanoparticles. In lipid-based carriers such as liposomes and NLCs, a PDI  $<0.3$  is considered acceptable and indicates monodispersity.<sup>38</sup> Thus, the nanosized (approximately 140 nm) RDS-NLC was homogeneously manufactured in this study.

Zeta potential is the electrical potential at the shear plane and indicates the degree of electrostatic repulsion. Both positively and negatively charged nanoparticles have advantages; for example, positively charged nanoparticles show a strong electrostatic interaction with mucus, which is negatively charged.<sup>39</sup> However, positively charged nanoparticles may increase cytotoxicity.<sup>40,41</sup> Neutral or slightly negatively charged nanoparticles have been shown to significantly prolong circulating time in the bloodstream and clear more slowly after an IV injection of nanoparticles.<sup>42,43</sup> In this study, we aimed to develop an RDS-NLC for IV injection, and the zeta-potentials of the blank-NLCs and RDS-NLC were  $-6.41 \pm 0.94$  and  $-6.84 \pm 0.59$  mV, respectively (Figure 1c). Therefore, the RDS-NLCs would remain in the bloodstream for a longer time than RDS would. Collectively, our results indicate that the negatively charged spherical nanosized RDS-NLCs may enhance cellular uptake and circulation time in the body.

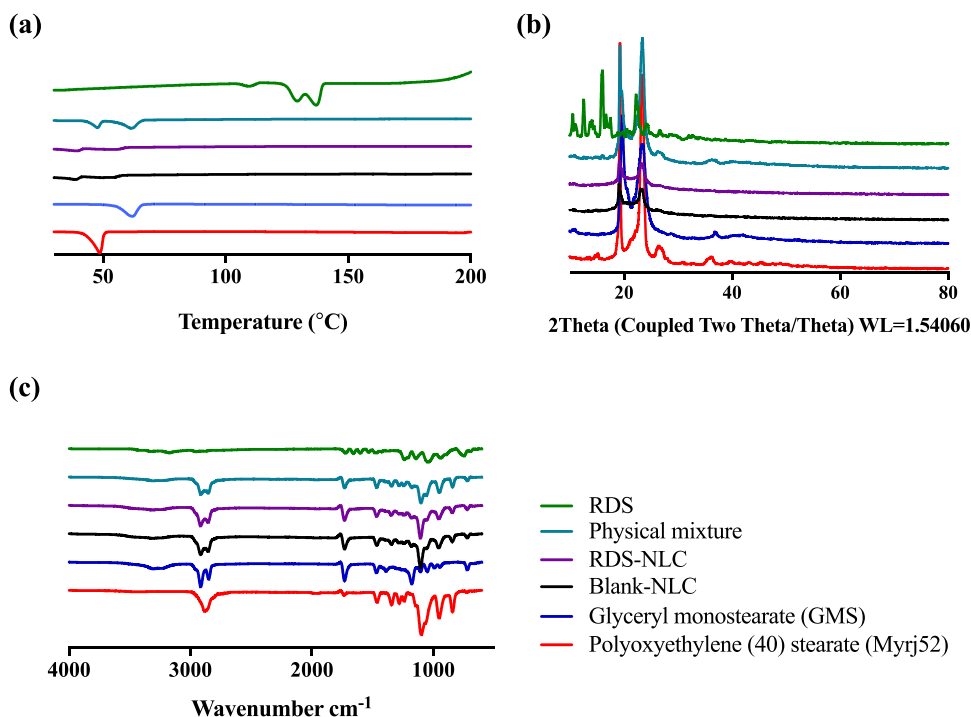


**Figure 2** Physicochemical properties of RDS-NLC. (a) Differential scanning calorimetry (DSC) thermogram. (b) X-ray diffraction (XRD) pattern. (c) Fourier transform-infrared spectroscopy (FT-IR) of RDS, physical mixture, glycerol monostearate (GMS), Myrj52, Blank-NLC, and RDS-NLC.

### Differential Scanning Calorimetry, Fourier Transform-Infrared Spectroscopy, and X-Ray Diffraction Analyses of Remdesivir-Loaded Nanostructured Lipid Carriers

Encapsulation efficiency (EE) is an important therapeutic and economic parameter that can affect drug efficiency; therefore, the production method should be optimized to maximize EE.<sup>44</sup> The EE value of the RDS-NLC was calculated to be 99.94%, indicating that almost all RDSs were entrapped into the NLC.

To evaluate the thermodynamic variations of RDS-NLC, we assessed the DSCs of RDS, blank-NLC, RDS-NLC, and NLC ingredients. RDS showed peaks at 129°C and 137°C, and endothermic peaks of NLC ingredients were observed at 62°C and 48°C for GMS and Myrj52, respectively (Figure 2a). When the DSC of the RDS-NLC and blank-NLC were measured, the endothermic peaks of the RDS, GMS, and Myrj52 were not observed, suggesting that the crystal structures of the lipids and surfactants were modified by the NLC. Moreover, the RDS was completely solubilized in the NLCs as the RDS peak was not observed in the RDS-NLCs, indicating that the crystallinity of the RDS was significantly decreased with NLCs.

To confirm the changes in the RDS crystallinity, we evaluated the XRD pattern of the RDS-NLCs. Figure 2b displays the XRD patterns of the RDS, RDS-NLC, blank-NLC, and NLC ingredients. For the ingredients, sharp peaks of the lipid and surfactant were observed at  $2\theta$  of 19° and 23°, and these peak intensities decreased in the RDS-NLC and Blank-NLC. This indicates that the crystallinity of the lipid and surfactant was lowered in the NLCs, reflecting the less-ordered structure of the ingredients. Moreover, RDS peaks were not detected in RDS-NLCs, indicating that RDS was stabilized in an amorphous form in NLCs. Therefore, RDS was successfully entrapped in the lipid cores of the NLCs.

We evaluated the potential interactions between RDS and the ingredients using FT-IR spectroscopy. FT-IR is used to reveal the surface adsorption of functional groups on nanoparticles.<sup>45</sup> FT-IR spectra are displayed in Figure 2c. RDS showed a peak at 3171  $\text{cm}^{-1}$ , indicating N-H stretching. GMS showed peaks for O-H, C-H, and C=O were observed at 2914, 2849, and 1729  $\text{cm}^{-1}$ , respectively. Moreover, these peaks were assigned to the physical mixture, blank-NLCs, and RDS-NLCs. The peak corresponding to C=O (1729  $\text{cm}^{-1}$ ) was reduced in the RDS-NLCs compared to that in GMS, indicating that RDS was entrapped in lipid matrices, such as GMS and Myrj52. In addition, there were no specific or new bands in RDS-NLCs, indicating the absence of chemical interactions. Collectively, these results indicate that RDS was encapsulated in the amorphous form in NLC and dissolved in lipid matrices.

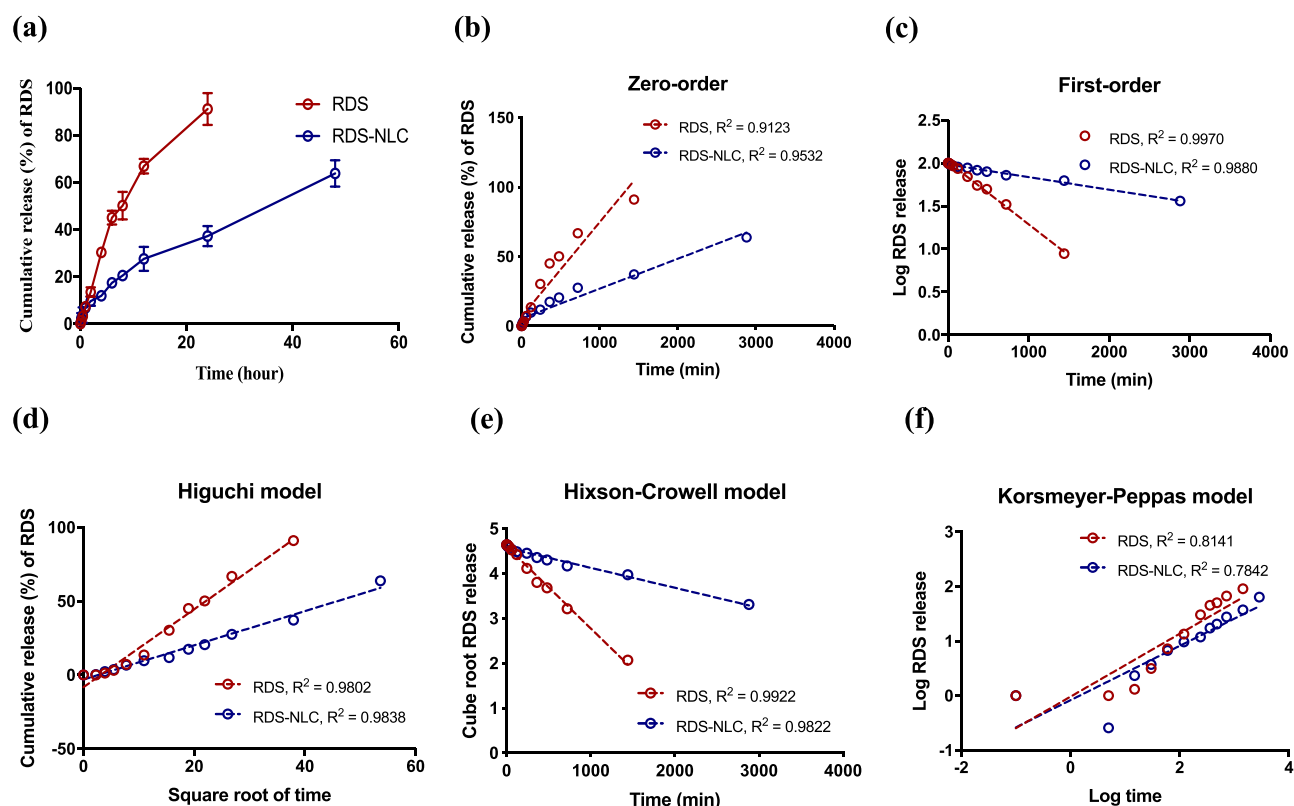


**Figure 3** In vitro release profiles of RDS and RDS-NLC. (a) Cumulative release of RDS from RDS and RDS-NLC in PBS containing 2 w/v% SLS (pH 7.4). (b–f) Release kinetic model fitness of RDS and RDS-NLC using zero-order, first-order, Higuchi-, Hixson-Crowell, and Korsmeyer-Peppas models.

## In vitro Release of Remdesivir-Loaded Nanostructured Lipid Carriers

Drug release is an important factor in evaluating the extent and rate of drug availability in the body. Therefore, the evaluation of drug release kinetics helps predict the effective maintenance level of drugs in the body. To reveal the in vitro and in vivo correlation, the release kinetics should be assessed with appropriate mathematical models.<sup>46</sup> Thus, the release mechanism of RDS-NLCs was evaluated using mathematical models, such as the zero-order, first-order, Higuchi, Hixson-Crowell, and Korsmeyer-Peppas models.

The release profiles of RDS and RDS-NLC are shown in Figure 3. In a PBS (pH 7.4) medium containing 2 w/v% SLS, the cumulative release values of RDS and RDS-NLC were  $91.12 \pm 6.76$  and  $37.21 \pm 4.22\%$ , respectively, at 24 h (Figure 3a), and  $63.75 \pm 5.65\%$  of RDS-NLC was released at 48 h. RDS-NLCs showed a sustained release property compared to RDS. When the release profile of RDS was fitted using mathematical models, the R<sup>2</sup> values for the zero-order, first-order, Higuchi, Hixson-Crowell, and Korsmeyer-Peppas models were 0.91, 0.99, 0.98, 0.99, and 0.81, respectively. Based on these values, the first-order model showed the best fit for RDS. Moreover, the first-order model was the most suitable for describing the release pattern of RDS-NLCs. Based on first-order kinetics, the release rate is concentration-dependent, indicating that the released amount of drug tends to decrease over time.<sup>47</sup> This means that the released RDS from RDS-NLC is proportional to the amount of RDS remaining in NLC. Therefore, the RDS-NLCs showed a sustained release profile, which was proportional to the decrease in RDS over time.

## In vitro Antiviral Activity of Remdesivir-Loaded Nanostructured Lipid Carriers Against SARS-CoV-2 and Variants in Vero Cells

To compare the antiviral activity of RDS and RDS-NLCs against SARS-CoV-2, drug dose-response curve analyses were performed in Vero E6 cells using a CPE-based assay (Figure 4a). In SARS-CoV-2 infected Vero cells, RDS and RDS-NLC demonstrated potent antiviral activity with EC<sub>50</sub> values of 1.6  $\mu$ M and 0.16  $\mu$ M, respectively.

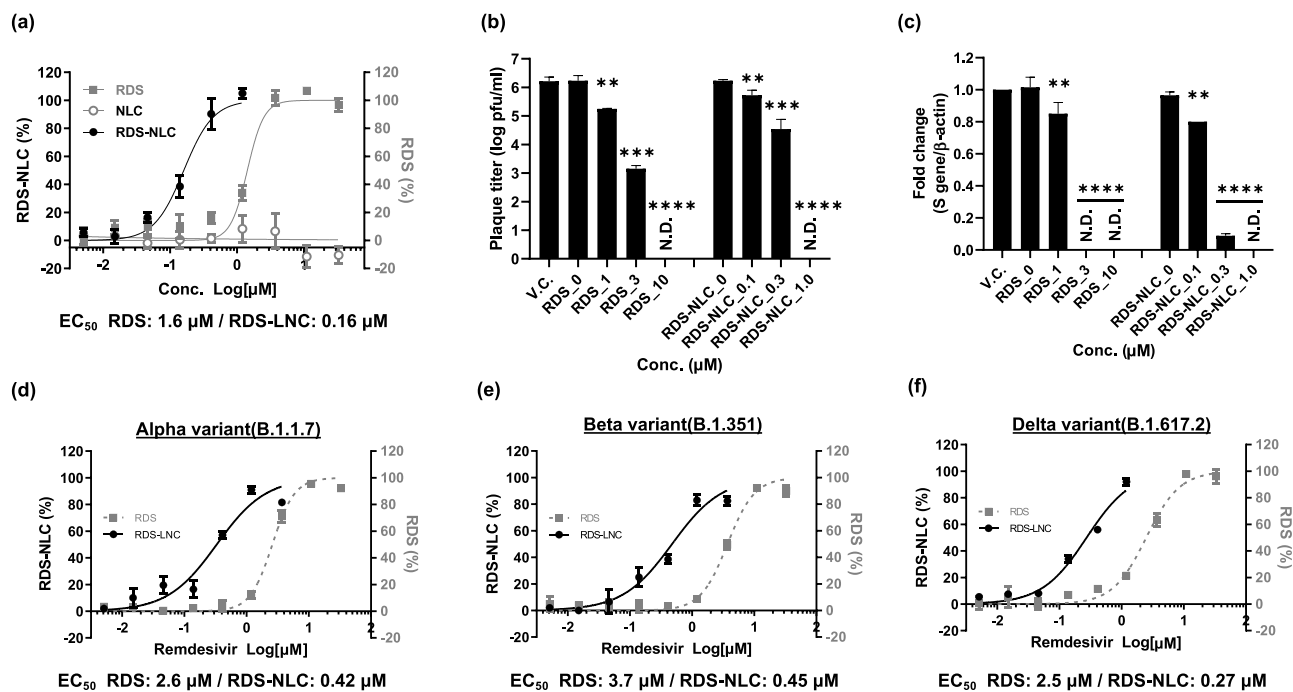


**Figure 4** Antiviral effects of RDS and RDS-NLC against SARS-CoV-2 and variants. (a) Antiviral effect of RDS and RDS-NLC in SARS-CoV-2 infected Vero cells. (b) Comparison of plaque titer between various concentrations of RDS and RDS-NLC. (c) Quantification of viral RNA (S-protein) after treatment with various concentrations of RDS or RDS-NLC. (d-f) Antiviral effects of RDS and RDS-NLC in SARS-CoV-2 alpha-, beta-, and delta-variants. Data are presented as mean  $\pm$  SD. \*\* $P < 0.01$  versus control. \*\*\* $P < 0.005$  versus control. \*\*\*\* $P < 0.0001$  versus control. Conc., concentration; RDS, remdesivir.

However, the Blank-NLC only treatment showed no antiviral activity. Similarly, dose-dependent inhibition of viral replication was determined using plaque assay and RT-qPCR (Figures 4b and c). Administration of 10 μM RDS and 1 μM RDS-NLC resulted in total suppression of viral particle production, whereas 1 μM RDS and 0.1 μM RDS-NLC resulted in a minimal reduction of viral titers. Consistent with the reduction in viral titers, a dose-dependent reduction in the intracellular viral genome was detected by RT-qPCR in Vero cells treated with RDS or RDS-NLC. Complete inhibition of intracellular viral mRNA synthesis was observed following treatment with either 10 μM RDS, and 1 μM RDS-NLC. To test the broad-spectrum activity of RDS and RDS-NLCs against SARS-CoV-2 variants, drug dose-response curve analyses were performed against alpha-, beta-, and delta- SARS-CoV-2 variants (Figure 4d). In Vero cells infected with SARS-CoV-2 variants, RDS and RDS-NLC demonstrated antiviral activity with  $EC_{50}$  values of 2.6 μM and 0.42 μM for alpha-variants, 3.7 μM and 0.45 μM for beta-variants, and 2.5 μM and 0.27 μM for delta-variants, respectively (Figure 4e and f). Notably, RDS-NLCs exhibited a 10-fold higher activity than RDS. Taken together, these data indicate that RDS-NLCs inhibit SARS-CoV-2 and variant infection in Vero cells by reducing the production of infectious viral particles and the synthesis of viral RNA significantly more efficiently than RDS does.

## Evaluation of the Cellular Uptake of Remdesivir-Loaded Nanostructured Lipid Carriers

To evaluate the cellular uptake of RDS-NLCs in Vero cells, we first evaluated intercellular RDS-NLCs using fluorescence microscopy and FAC, and then quantified RDS metabolites in Vero cells. Fluorescent images after treatment with the labeled RDS-NLCs and C6 solution are shown in Figure 4a. A small amount of C6 solution (green signal) was observed in Vero cells after treatment with C6 solution for 24 h. In contrast, an RDS-NLC signal was observed in the cytoplasm of Vero cells after RDS-NLC treatment (Figure 5a), indicating that RDS-NLCs were condensed and localized in the cytoplasm. Moreover, FAC analysis revealed that RDS-NLCs showed a higher fluorescence intensity than the C6 solution (Figure 5b).

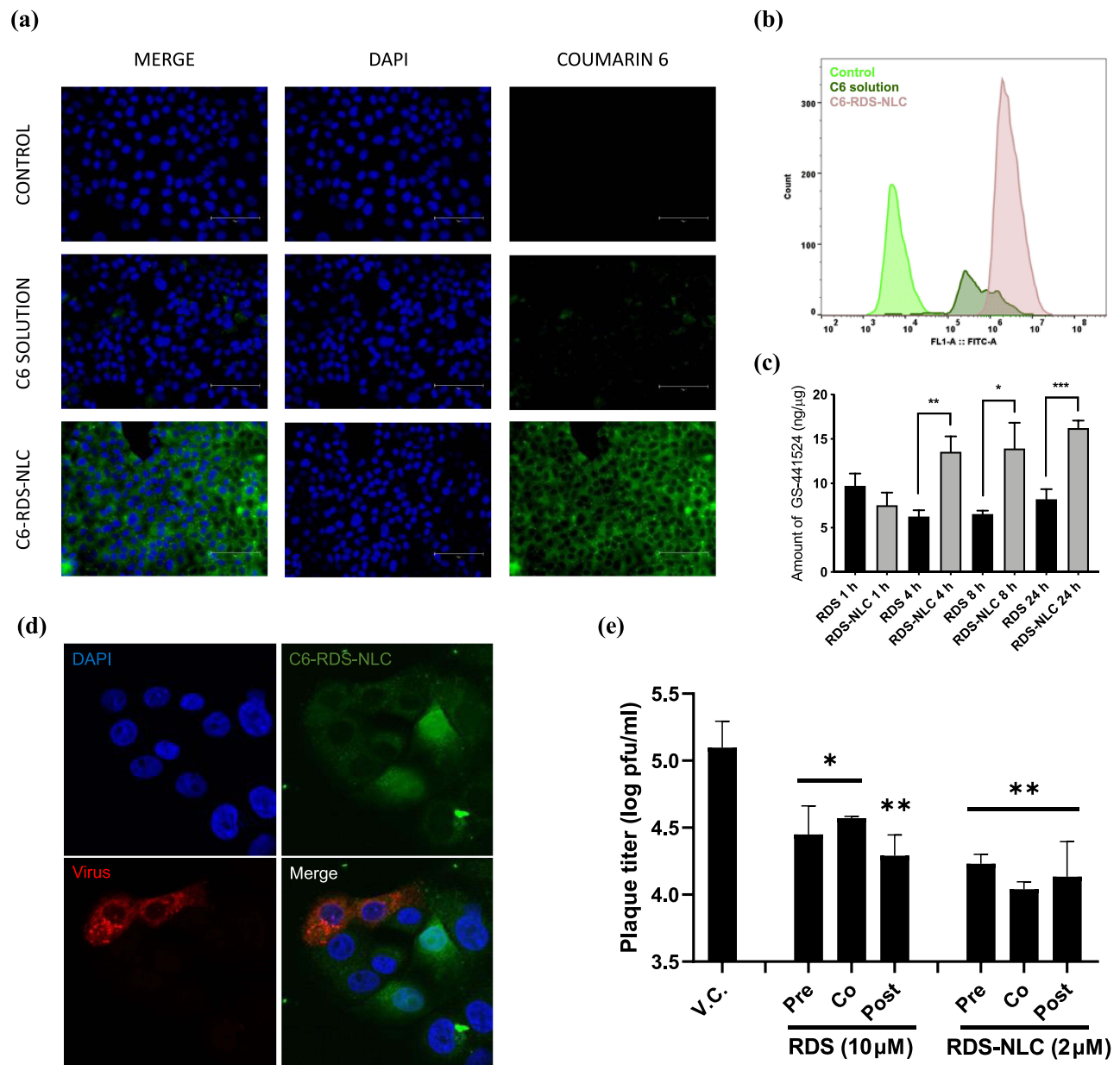


**Figure 5** Cellular uptake of RDS-NLC. (a) Fluorescent images of RDS-NLC (C6 labeled RDS-NLC, green signal) in Vero cells after 24 h of treatment. (b) Flow cytometry histograms of C6 solution (red) and RDS-NLC (green). Cells were incubated for 24 h. (c) Normalized amount of RDS metabolite (GS-441524) after treatments with RDS or RDS-NLC in Vero cells. (d) Immunofluorescent images of C6 labeled RDS-NLC in SARS-CoV-2 infected Vero cells. (e) Viral titer after treatment with RDS or RDS-NLC at different time points [pre-treatment (-2 h), co-treatment (0 h), and post-treatment (2 h)] in SARS-CoV-2 infected Vero cells. Data are presented as mean  $\pm$  SD. \* $P < 0.05$ . \*\* $P < 0.01$ . \*\*\* $P < 0.005$ .

To compare the differences in uptake between RDS and RDS-NLCs, the amount of RDS uptake in Vero cells was quantified after treatment with RDS or RDS-NLCs. RDS is extensively metabolized to active metabolites, such as alanine metabolite (GS-704277), nucleoside monophosphate, and active nucleoside triphosphate.<sup>48</sup> The nucleoside monophosphate is then dephosphorylated to form the nucleoside analog, GS-441524, which is the predominant circulating metabolite in plasma.<sup>10,49</sup> Therefore, we determined the amount of nucleoside analog (GS-441524) to assess the intercellular uptake of RDS and RDS-NLC. Figure 5c illustrates the amount of GS-441524 after RDS or RDS-NLC treatments in Vero cells. In the RDS group, the amount of GS-441524 peaked at 1 h, then decreased, and remained constant over time (4, 8, and 24 h). In contrast, the internalization of RDS-NLC increased and was maintained over time, indicating that RDS-NLC has a lag phase for cellular uptake. The uptake in the RDS-NLC group was significantly higher

than that in the RDS group at 4, 8, and 24 h. RDS is adapted from ProTide (prodrug approach) to enhance transmembrane diffusion.<sup>50</sup> Therefore, RDS can cross the cell membrane by simple diffusion. In contrast, nanoparticles, including NLC, are internalized in the cell via different endocytic pathways.<sup>51</sup> We confirmed that RDS-NLC and RDS were transported into the cell differently, and showed that NLC enhances both the cellular uptake and retention of RDS in the cell.

To evaluate the intracellular distribution of RDS-NLC in SARS-CoV-2 infected Vero cells, a cellular uptake assay was performed. The confocal microscopic images revealed that RDS-NLCs were present in the cytoplasm but not in the nucleus, even under viral infection conditions (Figure 5d). NLC enhanced the intercellular uptake and retention of RDS in the cell; thus, it can potentially improve antiviral efficacy and safety by reducing the clinical dose of RDS.

## Effect of Remdesivir-Loaded Nanostructured Lipid Carriers on the Life Cycle of SARS-CoV-2

To determine which step of the life cycle of SARS-CoV-2 was affected by RDS and RDS-NLCs, Vero cells were infected with SARS-CoV-2 and treated with RDS or RDS-NLCs. The viral titers were then quantified at different time points: pre-treatment (−2 h), co-treatment (0 h), and post-treatment (2 h). As shown in Figure 5e, the RDS treatments before and after infection resulted in similar viral titers, whereas the co-treatment showed a slightly higher viral titer. In contrast, the viral titer of the RDS-NLCs infected with SARS-CoV-2 was significantly lower at co-treatment than pre- or post-treatment. These results suggest that RDS-NLCs interact directly with viral particles or entry, and this effect may be mediated by NLC. Because the virus membrane originates in the cell phospholipid bilayer membrane, the presence of NLC particles in the extracellular space allows NLCs to interact with both viral particles and cell surface membranes. Additional studies are needed to further evaluate NLC-associated antiviral effects.

## Pharmacokinetics of Remdesivir-Loaded Nanostructured Lipid Carriers

We evaluated the pharmacokinetics of RDS-NLCs by injecting RDS and RDS-NLCs in rats. After IV injections of RDS or RDS-NLC at a dose of 10 mg/kg, the plasma concentration of the RDS metabolite was determined by UPLC-MS/MS. The time vs plasma concentration plot is illustrated in Figure 6. RDS was not detected in the plasma after RDS or RDS-NLCs injections in rats. As shown in Figure 5, GS-441524 was detectable in the plasma for up to 12 h in both the RDS and RDS-NLC groups. Remarkably, the GS-441524 plasma concentration in the RDS-NLC group was superior to that in the RDS group for 12 h. Moreover, a comparison of the pharmacokinetic parameters of the RDS and RDS-NLCs (Table 2) revealed that the  $C_{max}$  and area under the curve (AUC)<sub>0–24</sub> in the RDS-NLC group were approximately 2.3 and 2.1 fold higher than those in the RDS group, respectively, whereas the CI/F ratio was significantly decreased in the RDS-NLC group. Therefore, RDS-NLCs were better absorbed than RDS, and the NLCs increased the bioavailability of RDS by approximately 211%.

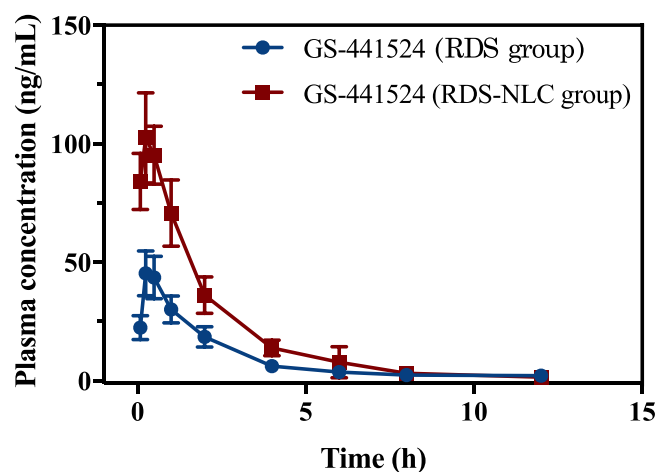


Figure 6 Plasma concentration of GS-441524 after the injection of RDS (circle) and RDS-NLC (square) injections (10 mg/kg) in rats.

**Table 2** Pharmacokinetic Parameters After RDS and RDS-NLC Injections (10 Mg/Kg) in Rats

Parameters	Unit	RDS	RDS-NLC
$T_{1/2\lambda z}$	hr	4.04 ± 2.92	3.07 ± 1.31
$T_{max}$	hr	0.33 ± 0.13	0.22 ± 0.07
$C_{max}$	ng/mL	46.32 ± 8.68	104.53 ± 17.68***
$AUC_{0-24}$	hr ng/mL	111.91 ± 16.89	234.77 ± 33.79***
V/F	L/kg	452.78 ± 277.88	192.12 ± 102.10
Cl/F	L/hr/kg	81.83 ± 54.56	41.99 ± 5.62***

Note: \*\*\* $p < 0.001$ .

Abbreviations:  $T_{1/2\lambda z}$ , half-life of the terminal portion of the curve;  $T_{max}$ , time at the maximum drug concentration;  $C_{max}$ , maximum plasma drug concentration;  $AUC_{0-24}$ , area under the curve from 0 to the end; V/F, volume of distribution during the elimination phase; Cl/F, body clearance during the elimination phase.

## Conclusion

In this study, we developed and evaluated RDS-loaded NLCs to assess their potential use as carriers, and evaluated the carrier effect to elucidate the impact of NLC on the life cycle of SARS-CoV-2. We demonstrated that NLC technology enhances the antiviral efficacy of RDS by improving its cellular uptake, retention, and bioavailability in vivo. In addition, NLC inhibited SARS-CoV-2 entry into the cell, thereby potentiating the antiviral efficacy of RDS. Although further studies are needed to further evaluate NLC-associated antiviral effects, the NLCs interacted directly with viral particles or entry. Therefore, the NLC showed the prophylactic effect against SARS-CoV-2. Thus, the application of NLC against SARS-CoV-2 may be a beneficial strategy for improving the antiviral effects of antiviral agents as well as preventing SARS-CoV-2 infection. However, further mechanism study is needed to clarify the prophylactic effect of NLC against SARS-CoV-2.

## Acknowledgments

SARS-CoV-2 (NCCP Nos. 43328, 43381, 43382, and 43390) was provided by the National Culture Collection for Pathogens (Korea National Institute of Health). This work was supported by the Basic Science Research Program (2019R1A2C1086102) of the National Research Foundation of Korea (NRF). We would like to acknowledge financial support from the Korea Institute of Toxicology (KIT, Korea) grant funded by the Ministry of Science and ICT (MIST, Korea) (Project number: KK-2210-01). This research was supported by the Ministry of Science and ICT (National Research Foundation of Korea [grant number NRF-2020M3A9I210856412 to JSS, EJ, and DH], Republic of Korea), and KRICT intramural funding (grant number SI-2232-20 to JSS, EJ, and DH, Republic of Korea).

## Disclosure

The authors declare that they have no known competing financial interests or personal relationships that could have influenced the work reported in this study.

## References

1. Wang C, Horby PW, Hayden FG, Gao GF. A novel coronavirus outbreak of global health concern. *Lancet*. 2020;395(10223):470–473. doi:10.1016/S0140-6736(20)30185-9
2. World Health Organization. Coronavirus (COVID-19) Dashboard. Available from: <https://covid19.who.int>. Accessed March 14, 2023.
3. Huang Y, Yang C, Xu XF, et al. Structural and functional properties of SARS-CoV-2 spike protein: potential antivirus drug development for COVID-19. *Acta Pharmacol Sin*. 2020;41(9):1141–1149. doi:10.1038/s41401-020-0485-4
4. Letko M, Marzi A, Munster V. Functional assessment of cell entry and receptor usage for SARS-CoV-2 and other lineage B betacoronaviruses. *Nat Microbiol*. 2020;5(4):562–569. doi:10.1038/s41564-020-0688-y
5. Tavakol S, Tavakol H, Alavijeh MS, Seifalian A. Can we succeed in the fight against SARS-CoV-2 with its emerging new variants? *Curr Pharm Design*. 2022;28:2953–2964. doi:10.2174/1381612828666220506142117

6. Simonis A, Theobald SJ, Fatkenheuer G, et al. A comparative analysis of remdesivir and other repurposed antivirals against SARS-CoV-2. *EMBO Mol Med.* 2021;13(1):e13105. doi:10.15252/emmm.202013105
7. Rao L, Xia S, Xu W, et al. Decoy nanoparticles protect against COVID-19 by concurrently adsorbing viruses and inflammatory cytokines. *Proc Natl Acad Sci USA.* 2020;117(44):27141–27147. doi:10.1073/pnas.2014352117
8. Moore JB, June CH. Cytokine release syndrome in severe COVID-19. *Science.* 2020;368(6490):473–474. doi:10.1126/science.abb8925
9. McCreary EK, Pogue JM. Coronavirus disease 2019 treatment: a review of early and emerging options. *Open Forum Infect Dis.* 2020;7(4):ofaa105. doi:10.1093/ofid/ofaa105
10. Jorgensen SCJ, Kebriaei R, Dresser LD. Remdesivir: review of pharmacology, pre-clinical data, and emerging clinical experience for COVID-19. *Pharmacotherapy.* 2020;40(7):659–671. doi:10.1002/phar.2429
11. Wang M, Cao R, Zhang L, et al. Remdesivir and chloroquine effectively inhibit the recently emerged novel coronavirus (2019-nCoV) in vitro. *Cell Res.* 2020;30(3):269–271. doi:10.1038/s41422-020-0282-0
12. Choy KT, Wong AYL, Kaewpreedee P, et al. Remdesivir, lopinavir, emetine, and homoharringtonine inhibit SARS-CoV-2 replication in vitro. *Antiviral Res.* 2020;178:104786. doi:10.1016/j.antiviral.2020.104786
13. Xia S, Zhu Y, Liu M, et al. Fusion mechanism of 2019-nCoV and fusion inhibitors targeting HR1 domain in spike protein. *Cell Mol Immunol.* 2020;17(7):765–767. doi:10.1038/s41423-020-0374-2
14. Wang C, Li W, Drabek D, et al. A human monoclonal antibody blocking SARS-CoV-2 infection. *Nat Commun.* 2020;11(1):2251. doi:10.1038/s41467-020-16256-y
15. Tanaka T, Narazaki M, Kishimoto T. Immunotherapeutic implications of IL-6 blockade for cytokine storm. *Immunotherapy.* 2016;8(8):959–970. doi:10.2217/imt-2016-0020
16. Tavakol S, Tavakol H, Alavijeh MS, Seifalian A. The world against versatile SARS-Cov-2 nanomachines: mythological or reality? *Curr Stem Cell Res.* 2021;T17:43–57.
17. Drugs. Coronavirus (COVID-19). Available from: <https://www.fda.gov/drugs/emergency-preparedness-drugs/coronavirus-covid-19-drugs>. Accessed March 14, 2023.
18. Brown AJ, Won JJ, Graham RL, et al. Broad spectrum antiviral remdesivir inhibits human endemic and zoonotic deltacoronaviruses with a highly divergent RNA dependent RNA polymerase. *Antiviral Res.* 2019;169:104541. doi:10.1016/j.antiviral.2019.104541
19. Cho A, Zhang L, Xu J, et al. Synthesis and characterization of 2'-C-Me branched C-nucleosides as HCV polymerase inhibitors. *Bioorg Med Chem Lett.* 2012;22(12):4127–4132. doi:10.1016/j.bmcl.2012.04.065
20. Lo MK, Jordan R, Arvey A, et al. GS-5734 and its parent nucleoside analog inhibit Filo-, Pneumo-, and Paramyxoviruses. *Sci Rep.* 2017;7:43395. doi:10.1038/srep43395
21. Yin W, Mao C, Luan X, et al. Structural basis for inhibition of the RNA-dependent RNA polymerase from SARS-CoV-2 by remdesivir. *Science.* 2020;368(6498):1499–1504. doi:10.1126/science.abc1560
22. Gordon CJ, Tchesnokov EP, Woolner E, et al. Remdesivir is a direct-acting antiviral that inhibits RNA-dependent RNA polymerase from severe acute respiratory syndrome coronavirus 2 with high potency. *J Biol Chem.* 2020;295(20):6785–6797. doi:10.1074/jbc.RA120.013679
23. Summary on compassionate use Remdesivir Gilead. European medicines agency 2020, EMA/178637/2020– rev.2; 2020.
24. Sahakijpijarn S, Moon C, Koleng JJ, et al. Development of Remdesivir as a dry powder for inhalation by thin film freezing. *Pharmaceutics.* 2020;12(11):1002. doi:10.3390/pharmaceutics12111002
25. Mohammadi MR, Nojoomi A, Mozafari M, et al. Nanomaterials engineering for drug delivery: a hybridization approach. *J Mater Chem B.* 2017;5(22):3995–4018. doi:10.1039/C6TB03247H
26. Muller RH, Radtke M, Wissing SA. Nanostructured lipid matrices for improved microencapsulation of drugs. *Int J Pharm.* 2002;242(1–2):121–128. doi:10.1016/S0378-5173(02)00180-1
27. Varahachalam SP, Lahooti B, Chamaneh M, et al. Nanomedicine for the SARS-CoV-2: state-of-the-art and future prospects. *Int J Nanomed.* 2021;16:539–560. doi:10.2147/IJN.S283686
28. Bhattacharjee R, Dubey AK, Ganguly A, et al. State-of-art high-performance nano-systems for mutated coronavirus infection management: from lab to clinic. *Opennano.* 2022;8:100078. doi:10.1016/j.onano.2022.100078
29. Tiwari S, Juneja S, Ghosal A, et al. Antibacterial and antiviral high-performance nanosystems to mitigate new SARS-CoV-2 variants of concern. *Curr Opin Biomed Eng.* 2022;21:100363. doi:10.1016/j.cobme.2021.100363
30. Beija M, Salvayre R, Lauth-de Viguier N, et al. Colloidal systems for drug delivery: from design to therapy. *Trends Biotechnol.* 2012;30(9):485–496. doi:10.1016/j.tibtech.2012.04.008
31. Moghimi SM, Hunter AC, Murray JC. Long-circulating and target-specific nanoparticles: theory to practice. *Pharmacol Rev.* 2001;53(2):283–318.
32. Cabral H, Kataoka K. Multifunctional nanoassemblies of block copolymers for future cancer therapy. *Sci Technol Adv Mater.* 2010;11(1):014109. doi:10.1088/1468-6996/11/1/014109
33. Na YG, Huh HW, Kim MK, et al. Development and evaluation of a film-forming system hybridized with econazole-loaded nanostructured lipid carriers for enhanced antifungal activity against dermatophytes. *Acta Biomater.* 2020;101:507–518. doi:10.1016/j.actbio.2019.10.024
34. Danaei M, Dehghankhold M, Ataei S, et al. Impact of particle size and polydispersity index on the clinical applications of lipidic nanocarrier systems. *Pharmaceutics.* 2018;10(2):57. doi:10.3390/pharmaceutics10020057
35. Makhlof A, Werle M, Tozuka Y, et al. mucoadhesive nanoparticulate system for the simultaneous delivery of macromolecules and permeation enhancers to the intestinal mucosa. *J Control Release.* 2011;149(1):81–88. doi:10.1016/j.jconrel.2010.02.001
36. Feng SS, Ruan G, Li QT. Fabrication and characterizations of a novel drug delivery device liposomes-in-microsphere (LIM). *Biomaterials.* 2004;25(21):5181–5189. doi:10.1016/j.biomaterials.2003.12.013
37. Müller RH, Jacobs C, Kayser O. Nanosuspensions as particulate drug formulations in therapy. *Adv Drug Deliv Rev.* 2001;47(1):3–19. doi:10.1016/S0169-409X(00)00118-6
38. Honary S, Zahir F. Effect of Zeta potential on the properties of nano-drug delivery systems - a review (Part 2). *Trop J Pharm Res.* 2013;12(2):265–273.
39. Blanco E, Shen H, Ferrari M. Principles of nanoparticle design for overcoming biological barriers to drug delivery. *Nat Biotechnol.* 2015;33(9):941–951. doi:10.1038/nbt.3330
40. Amini Y, Amel Jamehdar S, Sadri K, et al. Different methods to determine the encapsulation efficiency of protein in PLGA nanoparticles. *Biomed Mater Eng.* 2017;28(6):613–620. doi:10.3233/BME-171705

41. González Moreno A, López Guerrero MM, Vereda Alonso E, et al. Development of a new FT-IR method for the determination of iron oxide. Optimization of the synthesis of suitable magnetic nanoparticles as sorbent in magnetic solid phase extraction. *New J Chem.* 2017;41(17):8804–8811. doi:10.1039/C7NJ01522D
42. Son G-H, Lee B-J, Cho C-W. Mechanisms of drug release from advanced drug formulations such as polymeric-based drug-delivery systems and lipid nanoparticles. *J Pharm Investig.* 2017;47(4):287–296. doi:10.1007/s40005-017-0320-1
43. Bruschi ML. *Strategies to Modify the Drug Release from Pharmaceutical Systems.* Woodhead Publishing; 2015.
44. Eastman RT, Roth JS, Brimacombe KR, et al. Remdesivir: a review of its discovery and development leading to human clinical trials for treatment of COVID-19. *ACS Cent Sci.* 2020;6(6):1009. doi:10.1021/acscentsci.0c00747
45. Humeniuk R, Mathias A, Cao H, et al. Safety, tolerability, and pharmacokinetics of remdesivir, an antiviral for treatment of COVID-19, in Healthy Subjects. *Clin Transl Sci.* 2020;13(5):896–906. doi:10.1111/cts.12840
46. Rasmussen HB, Jurgens G, Thomsen R, et al. Cellular uptake and intracellular phosphorylation of GS-441524: IMPLICATIONS FOR ITS EFFECTIVENESS AGAINST COVID-19. *Viruses.* 2021;13(7):1369. doi:10.3390/v13071369
47. Behzadi S, Serpooshan V, Tao W, et al. Cellular uptake of nanoparticles: journey inside the cell. *Chem Soc Rev.* 2017;46(14):4218–4244. doi:10.1039/C6CS00636A
48. Son GH, Na YG, Huh HW, et al. Systemic design and evaluation of ticagrelor-loaded nanostructured lipid carriers for enhancing bioavailability and antiplatelet activity. *Pharmaceutics.* 2019;11(5):222. doi:10.3390/pharmaceutics11050222
49. Kim JM, Chung YS, Jo HJ, et al. Identification of coronavirus isolated from a patient in Korea with COVID-19. *Osong Public Health Res Perspect.* 2020;11(1):3–7. doi:10.24171/j.phrp.2020.11.1.02
50. Shin JS, Jung E, Kim M, et al. Saracatinib inhibits Middle East respiratory syndrome-coronavirus replication in vitro. *Viruses.* 2018;10(6):283. doi:10.3390/v10060283
51. Choi SW, Shin JS, Park S-J, et al. Antiviral activity and safety of remdesivir against SARS-CoV-2 infection in human pluripotent stem cell-derived cardiomyocytes. *Antiviral Res.* 2020;184:104955. doi:10.1016/j.antiviral.2020.104955

International Journal of Nanomedicine

Dovepress

## Publish your work in this journal

The International Journal of Nanomedicine is an international, peer-reviewed journal focusing on the application of nanotechnology in diagnostics, therapeutics, and drug delivery systems throughout the biomedical field. This journal is indexed on PubMed Central, MedLine, CAS, SciSearch<sup>®</sup>, Current Contents<sup>®</sup>/Clinical Medicine, Journal Citation Reports/Science Edition, EMBase, Scopus and the Elsevier Bibliographic databases. The manuscript management system is completely online and includes a very quick and fair peer-review system, which is all easy to use. Visit <http://www.dovepress.com/testimonials.php> to read real quotes from published authors.

Submit your manuscript here: <https://www.dovepress.com/international-journal-of-nanomedicine-journal>